PROCEEDINGS — OF — **THE ROYAL SOCIETY** **A** | MATHEMATICAL, PHYSICAL & ENGINEERING SCIENCES

Dynamics of an electrostatically charged elastic rod in fluid

Sookkyung Lim, Yongsam Kim and David Swigon

References	**This article cites 38 articles, 3 of which can be accessed free** http://rspa.royalsocietypublishing.org/content/early/2010/08/18/rspa.2010.0174.full.html#ref-list-1
P<P	Published online 18 August 2010 in advance of the print journal.
Subject collections	Articles on similar topics can be found in the following collections computational physics (17 articles) computer modelling and simulation (55 articles) applied mathematics (236 articles)
Email alerting service	Receive free email alerts when new articles cite this article - sign up in the box at the top right-hand corner of the article or click **here**

Dynamics of an electrostatically charged elastic rod in fluid

By Sookkyung Lim[1,*], Yongsam Kim[2] and David Swigon[3]

[1]Department of Mathematical Sciences, University of Cincinnati,
839 Old Chem, Cincinnati, OH 45221, USA
[2]Department of Mathematics, Chung-Ang University,
Dongjakgu Heukseokdong, Seoul 156-756, Republic of Korea
[3]Department of Mathematics, University of Pittsburgh, 511 Thackeray Hall,
Pittsburgh, PA 15260, USA

We investigate the effects of electrostatic and steric repulsion on the dynamics of a pre-twisted charged elastic rod immersed in a viscous incompressible fluid. Equations of motion of the rod include the fluid–structure interaction, rod elasticity and a combination of two interactions that prevent self-contact, namely the electrostatic interaction and hard-core repulsion. The governing equations are solved using the generalized immersed-boundary method. We find that after perturbation, a pre-twisted minicircle collapses into a compact supercoiled configuration. The collapse proceeds along a complex trajectory that may pass near several unstable equilibrium configurations, before it settles in a locally stable equilibrium. The dwell time near an unstable equilibrium can be up to several microseconds. Both the final configuration and the transition path are sensitive to the initial excess link, ionic strength of the solvent and the initial perturbation.

1. Introduction

Modelling of many biological systems requires one to take into account the interaction of elastic structures with fluid. The immersed-boundary (IB) method (Peskin 2002), created to study the dynamics of heart valves (Peskin 1972), is an efficient mathematical procedure that has been used in the numerical simulation of a variety of such systems. The mathematical formulation of the IB method employs Eulerian independent variables for the description of the fluid and Lagrangian independent variables for the elastic solid. The interaction between the solid and the fluid is mediated by forces applied by the structure on the fluid and vice versa. Dirac delta functions are used to convert forces from one set of independent variables to the others. The numerical scheme for the IB method employs two meshes—a Cartesian mesh for Eulerian variables and a curvilinear mesh for Lagrangian variables, which moves freely through

*Author for correspondence (limsk@math.uc.edu).

1

the Cartesian mesh. Smoothed approximations of Dirac delta functions are involved in the interpolation between the two meshes. A distinguishing feature of the IB method is that the velocity of the structure is identical to the velocity of the surrounding fluid owing to no-slip conditions, i.e. the structure is carried by the fluid (Peskin & McQueen 1996; Peskin 2002).

The classical IB method is applicable to the dynamics of two- or three-dimensional structures in a three-dimensional fluid, but cannot be directly applied to a one-dimensional structure (a space curve) because of the presence of a singularity due to delta functions. The generalized IB method (Lim *et al.* 2008) resolves this issue by using a smoothed delta function with a compact support, which has the effect of assigning a cross-sectional radius to the space curve. In addition, the generalized IB method incorporates the special Cosserat rod theory and is distinguished by two new features: (i) the local angular velocity of the fluid at the IB is evaluated, along with the local linear velocity of the fluid, and (ii) the IB applies torque as well as force to the surrounding fluid. It was observed that the generalized IB method prevents the passage of a discretely modelled, infinitesimally thin elastic rod through itself, even without the use of explicit repulsive potentials (Lim *et al.* 2008). This effect appears to be the result of the no-slip condition at the fluid–structure interface, where the interpolated velocity field is continuous, as is also true in the classical IB method. Nonetheless, the prevention of self-penetration did not prove to be reliable in the numerical implementation, since it varied with the grid-spacing and the time step.

Here, we present an improved IB method for modelling the dynamics of elastic rod-like structures in a fluid. In this method, the self-contact is treated naturally by including two types of interactions: (i) a hard-core potential that does not allow two points on the axis of the rod to approach closer than the specified distance (rod diameter) and (ii) a long-range electrostatic repulsion. Inclusion of these interactions prevents the passage of the rod through itself and enables one to study the effects of the rod diameter and the magnitude of the repulsive force on the dynamics.

The inclusion of electrostatic force was motivated by our application of the model to the dynamics of short DNA molecules in a solvent. DNA is a double-stranded molecule composed of two polynucleotide strands that are bound together by hydrogen bonds between complementary nucleotide bases. In normal conditions, the strands wind around the DNA axis as two right-handed helices with diameters of 2 nm and pitches of 3.57 nm. During biological processes, such as transcription or replication, various mechanical forces act on the DNA and cause its underwinding or overwinding, i.e. an increase or decrease in the helical pitch. The molecule responds by releasing some of the stored twisting energy through a deformation that results in the so-called supercoiled configurations (Bates & Maxwell 1993).

Aside from the bending and torsional elasticity, the dynamics of the molecule is influenced by long-range electrostatic interactions between charged phosphate residues on the DNA backbone. Two of these residues are located every 0.34 nm, each carrying one electronic charge. The main influence of these charges is that the chance of self-contact of the DNA, i.e. contact of a point on the surface of the DNA with another point on the surface, is greatly reduced as the electrostatic repulsion provides a cushion between any two closely approaching DNA segments.

Electrostatic interaction is particularly important for supercoiled DNA dynamics because, upon supercoiling, many parts of the double helix come into close contact. A secondary effect of electrostatics is the so-called electrostatic stiffening of the molecule, i.e. increased resistance to bending (Odijk 1977; Skolnick & Fixman 1977; Baumann *et al.* 1997).

The electrostatic interaction between DNA charges in solution is screened by counterions, and hence the strength of any electrostatic effect decreases with increasing ionic strength of the solvent, i.e. the concentration of dissolved salt. There are several theories describing the extent of such screening. The most commonly employed is the theory of counterion condensation, due to Manning (1978), which concludes that the DNA is surrounded by a concentrated layer of counterions that neutralizes about 76 per cent of the DNA charge. The electrostatic energy is then described by a Debye–Hückel term as a function of the modified charge, molar salt concentration and the distance between the charges.

Equilibrium configurations of supercoiled circular DNA have been studied extensively using elastic-rod models (e.g. Le Bret 1979, 1984; Benham 1989; Yang *et al.* 1993; Tobias *et al.* 1994; Coleman *et al.* 1995, 2000; Westcott *et al.* 1995; Dichmann *et al.* 1996 and also references in Swigon 2009). Schlick *et al.* (1994) incorporated both elastic potential and electrostatic forces in a computational model of DNA that represented the molecule by cubic B-splines. They found that at low salt, the electrostatic term dominates over the bending and twisting terms and the DNA assumes more open configurations, while at high salt, the DNA structure is dominated by the bending term and takes upon compact and bent interwound configurations. Westcott *et al.* (1997) also studied the mechanical equilibria of charged DNA by solving the equations of mechanical equilibrium for elastic DNA at fixed salt concentration. They showed that the extensible DNA yields the same equilibrium configurations as in the inextensible DNA. Recently, Biton *et al.* (2007) and Biton & Coleman (2010) have analysed the influence of electrostatic repulsion on configurations of both open and closed intrinsically curved DNA segments. The influence of electrostatics on DNA configurations in single-molecule manipulation experiments was recently analysed by Clauvelin *et al.* (2009) and Brutzer *et al.* (2010). The departure of a pre-twisted circular elastic rod from the circular equilibrium configuration has been studied using dynamical rod theories that included drag forces to represent the interaction of the rod with fluid (Klapper 1996; Goriely & Tabor 1997; Goyal *et al.* 2005, 2008).

We here use the generalized IB method to study the dynamics of supercoiling of a pre-twisted charged elastic rod and its dependence on the ionic strength of the surrounding solvent, mimicking the supercoiling of DNA minicircles. We model the solvent as a viscous incompressible fluid, assume a no-slip interaction between the solvent and the rod and treat the rod as a homogeneous, transversely isotropic, intrinsically straight and uniformly charged rod obeying special Cosserat theory of rods (Antman 1995), with electrostatic forces governed by the Debye–Hückel theory. The rod is initially circular with a uniform twist density and an imposed excess link corresponding to an integer number of turns of one end with respect to the other before closure. This configuration is perturbed in its twist density (but not the axial curve) and then left to evolve in accord with the governing equations.

2. Equations of motion

We consider a closed bent and twisted rod immersed in an incompressible fluid governed by the Navier–Stokes equations. The mathematical model discussed here is based on the model introduced by Lim *et al.* (2008) with electrostatic and steric repulsion forces included in addition to the elastic force. The immersed rod is represented by a three-dimensional closed space curve with an associated orthonormal triad at each point of the curve.

Eulerian coordinates are used in the description of the motion of the fluid, while Lagrangian variables are used to describe the immersed rod and its properties. The interaction between these two types of variables is facilitated by means of integral transformations that involve a smoothed version of the three-dimensional Dirac delta function (Peskin & McQueen 1996).

The coupled system of equations of the rod and the fluid is as follows:

$$\rho\left(\frac{\partial \mathbf{u}}{\partial t} + \mathbf{u} \cdot \nabla \mathbf{u}\right) = -\nabla p + \mu \nabla^2 \mathbf{u} + \mathbf{f}^{\mathrm{b}}, \tag{2.1}$$

$$\nabla \cdot \mathbf{u} = 0, \tag{2.2}$$

$$0 = \mathbf{f} + \frac{\partial \mathbf{F}}{\partial s}, \tag{2.3}$$

$$0 = \mathbf{n} + \frac{\partial \mathbf{N}}{\partial s} + \frac{\partial \mathbf{X}}{\partial s} \times \mathbf{F}, \tag{2.4}$$

$$\mathbf{F} = F^1 \mathbf{D}^1 + F^2 \mathbf{D}^2 + F^3 \mathbf{D}^3, \tag{2.5}$$

$$\mathbf{N} = N^1 \mathbf{D}^1 + N^2 \mathbf{D}^2 + N^3 \mathbf{D}^3, \tag{2.6}$$

$$N^1 = a_1 \frac{\partial \mathbf{D}^2}{\partial s} \cdot \mathbf{D}^3, \quad N^2 = a_2 \frac{\partial \mathbf{D}^3}{\partial s} \cdot \mathbf{D}^1, \quad N^3 = a_3 \frac{\partial \mathbf{D}^1}{\partial s} \cdot \mathbf{D}^2, \tag{2.7}$$

$$F^1 = b_1 \mathbf{D}^1 \cdot \frac{\partial \mathbf{X}}{\partial s}, \quad F^2 = b_2 \mathbf{D}^2 \cdot \frac{\partial \mathbf{X}}{\partial s}, \quad F^3 = b_3\left(\mathbf{D}^3 \cdot \frac{\partial \mathbf{X}}{\partial s} - 1\right), \tag{2.8}$$

$$\mathbf{f}^{\mathrm{b}}(\mathbf{x}, t) = \int \left(-\mathbf{f}(s, t)\right) \delta_c(\mathbf{x} - \mathbf{X}(s, t)) \, \mathrm{d}s + \frac{1}{2}\nabla \times \int (-\mathbf{n}(s, t))\delta_c(\mathbf{x} - \mathbf{X}(s, t)) \, \mathrm{d}s$$

$$+ \int (-\mathbf{f}^{\mathrm{c}}(s, t))\delta_c(\mathbf{x} - \mathbf{X}(s, t)) \, \mathrm{d}s + \sum_{i=1}^{n}(-\mathbf{f}^{\mathrm{e}}_i(t))\delta_c(\mathbf{x} - \mathbf{X}_i(t)), \tag{2.9}$$

$$\frac{\partial \mathbf{X}(s, t)}{\partial t} = \mathbf{U}(s, t) = \int \mathbf{u}(\mathbf{x}, t) \, \delta_c(\mathbf{x} - \mathbf{X}(s, t)) \, \mathrm{d}\mathbf{x}, \tag{2.10}$$

$$\mathbf{W}(s, t) = \frac{1}{2}\int (\nabla \times \mathbf{u})\delta_c(\mathbf{x} - \mathbf{X}(s, t)) \, \mathrm{d}\mathbf{x} \tag{2.11}$$

and
$$\frac{\partial \mathbf{D}^i(s, t)}{\partial t} = \mathbf{W}(s, t) \times \mathbf{D}^i(s, t), \quad i = 1, 2, 3, \tag{2.12}$$

where $\mathbf{f}^{\mathrm{c}}(s, t)$ and $\mathbf{f}^{\mathrm{e}}_i(t)$ are the steric repulsion and electrostatic forces defined below.

Equations (2.1) and (2.2) are the Navier–Stokes equations for the velocity $\mathbf{u}(\mathbf{x}, t)$ and pressure $p(\mathbf{x}, t)$ of an incompressible fluid; here, $\mathbf{x} = (x_1, x_2, x_3)$ describes a position in space and t is the time. The motion of the fluid is subject to the body force $\mathbf{f}^{\mathrm{b}}(\mathbf{x}, t)$, which here represents the force per unit volume applied to the fluid by the immersed rod. The constant parameters ρ and μ are the fluid density and the fluid viscosity, respectively.

The equilibrium equations (2.3)–(2.8) are employed to relate the force and torque of the immersed rod to the external forces applied on it, where the rod is defined by giving its axial curve $\mathbf{X}(s, t)$ and an orthonormal triad embedded in each cross section $(\mathbf{D}^1(s, t), \mathbf{D}^2(s, t), \mathbf{D}^3(s, t))$. The rod is assumed to have no dynamics of its own other than the one that follows the motion of the fluid. This approximation becomes exact in the limit of a thin elastic rod with density equal to the fluid density and no-slip conditions imposed on the fluid velocity at the rod surface. All variables in equations (2.3)–(2.8) are functions of the linear material coordinate s of the rod (not necessarily the arclength) and the time t. $\mathbf{F}(s, t)$ and $\mathbf{N}(s, t)$ are the force and moment (couple) transmitted across the section of the rod at s. The expressions $-\mathbf{f}(s, t)$ and $-\mathbf{n}(s, t)$ are the density of the external force and the torque applied by the rod on the fluid.
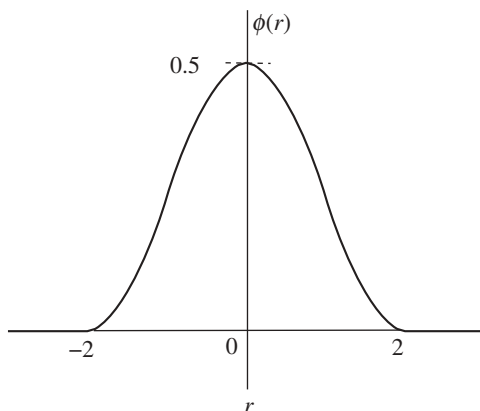
The internal force and moment on the perpendicular cross section, $\mathbf{F}$ and $\mathbf{N}$, and also the applied force density $\mathbf{f}$ and the torque density $\mathbf{n}$ may be expanded in the basis $(\mathbf{D}^1, \mathbf{D}^2, \mathbf{D}^3)$. Equations (2.7) and (2.8) are the constitutive relations of the special Cosserat theory of rods (Antman 1995). Here, a_1 and a_2 are the bending moduli of the rod about $\mathbf{D}^1$ and $\mathbf{D}^2$, respectively, and a_3 is the twisting modulus of the rod. The parameters b_1 and b_2 are the shear-force constants and b_3 is the stretch-force constant. The elastic energy of the rod is given by

$$E = \frac{1}{2} \int \left[a_1 \left(\frac{\partial \mathbf{D}^2}{\partial s} \cdot \mathbf{D}^3 \right)^2 + a_2 \left(\frac{\partial \mathbf{D}^3}{\partial s} \cdot \mathbf{D}^1 \right)^2 + a_3 \left(\frac{\partial \mathbf{D}^1}{\partial s} \cdot \mathbf{D}^2 \right)^2 \right.$$

$$\left. + b_1 \left(\mathbf{D}^1 \cdot \frac{\partial \mathbf{X}}{\partial s} \right)^2 + b_2 \left(\mathbf{D}^2 \cdot \frac{\partial \mathbf{X}}{\partial s} \right)^2 + b_3 \left(\mathbf{D}^3 \cdot \frac{\partial \mathbf{X}}{\partial s} - 1 \right)^2 \right] \mathrm{d}s. \qquad (2.13)$$

For simplicity, we assume that $a_1 = a_2 \equiv a$ and $b_1 = b_2 \equiv b$, which corresponds to the case of a rod with transversely isotropic material properties.

Equations (2.9)–(2.11) describe the interactions between the fluid and the rod. These interaction equations connect the Lagrangian and Eulerian variables via a three-dimensional smoothed Dirac delta function $\delta_c(\mathbf{x}) = \delta_c(x_1)\delta_c(x_2)\delta_c(x_3)$, which acts as a kernel of the integral transformations that appear in the interaction equations. The particular choice of $\delta_c(\mathbf{x})$ that we make in this work is the following:

$$\delta_c(\mathbf{x}) = \frac{1}{c^3} \phi\left(\frac{x_1}{c}\right) \phi\left(\frac{x_2}{c}\right) \phi\left(\frac{x_3}{c}\right), \qquad (2.14)$$

Figure 1. One-dimensional delta function $\phi(r)$.

where $\mathbf{x} = (x_1, x_2, x_3)$ and the function ϕ is given by

$$\phi(r) = \begin{cases} \dfrac{3 - 2|r| + \sqrt{1 + 4|r| - 4r^2}}{8}, & \text{if } |r| \leq 1, \\[3mm] \dfrac{5 - 2|r| - \sqrt{-7 + 12|r| - 4r^2}}{8}, & \text{if } 1 \leq |r| \leq 2, \\[3mm] 0, & \text{if } |r| \geq 2, \end{cases}$$

(figure 1). Note that $\delta_c(\mathbf{x} - \mathbf{X})$ is a continuous function of $\mathbf{x}$ with continuous first derivatives and with support equal to a cube of edge $4c$ centred on $\mathbf{X}$. Whenever c is an integer multiple of h, the function $\delta_c(\mathbf{x} - \mathbf{X})$ satisfies two identities that are of particular importance in this work. Note in particular that these identities hold for all $\mathbf{X}$,

$$\sum_{\mathbf{j}} \delta_c(\mathbf{j}h - \mathbf{X})h^3 = 1 \tag{2.15}$$

and

$$\sum_{\mathbf{j}} (\mathbf{j}h - \mathbf{X})\delta_c(\mathbf{j}h - \mathbf{X})h^3 = 0, \tag{2.16}$$

where $\mathbf{j}$ is any vector with integer components, and h is the meshwidth of the fluid grid. As mentioned above, these identities hold only if c/h is a positive integer, and we shall choose h so that this is the case. The above identities ensure that force and torque generated by the rod are correctly applied to the fluid by our numerical scheme.

In equation (2.9), the first term describes how the force of the rod acts on the fluid and the second term describes how the torque of the rod acts on the fluid (see Lim *et al.* 2008 for details).

The repulsive force $\mathbf{f}^c$ is included to prevent penetration of the rod surface. It is assumed to be a Hookian force proportional to the amount of penetration, i.e.

$$\mathbf{f}^c(s, t) = \sum_{s'} \mathbf{f}^c(s, s', t), \tag{2.17}$$

where

$$\mathbf{f}^c(s, s', t) = g(D - |\mathbf{X}(s, t) - \mathbf{X}(s', t)|) \frac{\mathbf{X}(s, t) - \mathbf{X}(s', t)}{|\mathbf{X}(s, t) - \mathbf{X}(s', t)|}, \tag{2.18}$$

for any two material points s and s', such that $|s - s'| > 2D$, $|\mathbf{X}(s, t) - \mathbf{X}(s', t)| \leq D$ and $(\mathbf{X}(s, t) - \mathbf{X}(s', t)) \cdot \mathbf{T}(s, t) = (\mathbf{X}(s, t) - \mathbf{X}(s', t)) \cdot \mathbf{T}(s', t) = 0$. (In practice, for any s there are only finitely many s' obeying such conditions, whence the sum in equation (2.17).) The constant $D = 20\,\text{Å}$ is the diameter of the DNA, and the constant g is chosen sufficiently large so that no significant penetration occurs.

Electrostatics is included in the external force $\mathbf{f}^b$ as a screened Coulombic force $\mathbf{f}^e_i$, defined by

$$\mathbf{f}^e_i(t) = \sum_{j \neq i}^{n} \mathbf{F}^e_{ij}(t), \tag{2.19}$$

where

$$\mathbf{F}^e_{ij}(t) = \frac{q_i q_j \mathrm{e}^{-\kappa d_{ij}(t)}}{4\pi\epsilon_0\epsilon_w d_{ij}(t)} \left(\frac{1}{d_{ij}(t)} + \kappa \right) \frac{(\mathbf{X}_i(t) - \mathbf{X}_j(t))}{d_{ij}(t)}, \tag{2.20}$$

where $\mathbf{X}_i$ and q_i are the position and net charge of the ith base pair, respectively, d_{ij} is the distance between net charges q_i and q_j and n is the number of base pairs. The constant ϵ_0 is the permittivity of free space and ϵ_w is the dielectric constant of water at $300\,\text{K}$. For simplicity, we represent each base pair by one charge located on the DNA axis. The condensed monovalent cations around the surface of the DNA reduce the charge of each phosphate group to $0.24e$, where e is the elementary charge of an electron (Manning 1978; Williams & Maher 2000). Since there are two such phosphate groups per base pair, q_i is $0.48e$. The Debye screening parameter, κ, is given by

$$\kappa = 0.329\sqrt{C_s}\,\text{Å}^{-1}, \tag{2.21}$$

where C_s is the molar salt concentration in moles per litre. The screened Coulombic force can be obtained as the first variation of the Debye–Hückel electrostatic potential (Westcott *et al.* 1997),

$$E_{\text{electro}} = \sum_{i<j} \frac{q_i q_j \mathrm{e}^{-\kappa d_{ij}}}{4\pi\epsilon_0\epsilon_w d_{ij}}. \tag{2.22}$$

Equation (2.10) represents the condition that the rod moves at the same velocity as the fluid, after averaging in a manner determined by the smoothed Dirac delta function. Equation (2.11) represents a similar relation between the angular velocity $\mathbf{W}(s, t)$ of the rod and a local average of the angular velocity of the fluid, $1/2(\nabla \times \mathbf{u})$. Again, the smoothed delta function is used to determine the appropriate weighted average of the local fluid velocity. The change in orientation of the triad at each point of the rod is given by equation (2.12).

Table 1. Computational parameters.

parameters	symbol	value
grid size	$N \times N \times N$	64^3
domain size	$L \times L \times L$	$L = 725\,\text{Å}$
time step	Δt	$1 \times 10^{-10}\,\text{s}$
fluid density	ρ	$1\,\text{g cm}^{-3}$
fluid viscosity	μ	$0.01\,\text{g}\,(\text{cm s})^{-1}$
permittivity of free space	ϵ_0	$3.45 \times 10^{-7}\text{e}^2/(g\,\text{Å}^3\,\text{s}^{-2})$
dielectric constant of water	ϵ_w	77.7
electric charge	q	$0.24 \times 2\text{e}$
molar salt concentration	C_s	$0.001 \sim 0.1\,\text{M}$
Debye screening parameter	κ	$0.329\sqrt{c_\text{s}}\,\text{Å}^{-1}$
bending modulus	$a_1 = a_2 = a$	$1.3 \times 10^{-19}\,\text{g cm}^3\,\text{s}^{-2}$
twist modulus	a_3	$1.82 \times 10^{-19}\,\text{g cm}^3\,\text{s}^{-2}$
shear-force constants	$b_1 = b_2 = b$	$5 \times 10^{-5}\,\text{g cm s}^{-2}$
stretch modulus	$b_3 = b$	$5 \times 10^{-5}\,\text{g cm s}^{-2}$
number of base pairs	n	600
radius	r	$324.676\,\text{Å}$

Any deformation of a closed DNA is subject to the constraint of a fixed linking number Lk, defined as one half of the number of signed crossings of a DNA strand and the DNA axis in a planar projection (Calladine *et al.* 2004). A related quantity is the excess link ΔLk, which is a topological invariant, just like Lk, and is equal to half of the number of signed crossings of the axial curve and the curve that is formed by the endpoints of the vector $\mathbf{D}^1$ that is embedded in the cross section, and is constant in a stress-free configuration. If the axial curve of closed DNA is a simple closed planar curve, then it follows from the theorem of White (1969, 1989) that

$$\Delta Lk = \Delta Tw = \int \frac{\text{d}\mathbf{D}^1}{\text{d}s} \cdot \mathbf{D}^2\,\text{d}s, \tag{2.23}$$

and hence ΔLk equals the total number of turns of one end of the rod before it is sealed with the other end to produce a ring.

The numerical scheme we employ to solve the system (2.1)–(2.12) and (2.17)–(2.20) is based on the generalized IB method. In particular, since the discretized Navier–Stokes equations are linear in the variables of time level $(n+1)$ with constant coefficients that depend on the variables at time level n, Fourier transformation decouples the discretized system into N^3 separate 4×4 systems of linear equations that are easily solved (for details, see Lim *et al.* 2008). The parameter values used in the computations are listed in table 1. The elastic and electrostatic constants are based on the physical properties of the DNA (Westcott *et al.* 1997). In particular, the ratio of twisting to bending moduli, a_3/a is here chosen to be 1.4 in accord with the experimental estimates obtained by measurements of the free energy of supercoiling for small DNA rings (Horowitz & Wang 1984) and single DNA manipulation experiments (Strick *et al.* 1996). Each trajectory was continued until the total kinetic energy of

the system dropped below $10^{-12}kT$ to make sure that the system converged to a locally stable equilibrium. The computation of one dynamical trajectory takes 2–3 days of CPU time on a common Linux workstation. The order of accuracy of the numerical method was verified by performing calculations on three different grid sizes of 64^3, 128^3 and 256^3, comparing the discrete L^2-norm of the difference in fluid velocities and computing the convergence ratios. For example, for the trajectory of the system with $(\Delta Lk, C_{\mathrm{s}}) = (4, 0.1\,\mathrm{M})$ (see below), the convergence ratios for the velocity $\mathbf{u} = (u, v, w)$ at $t = 0.4\,\mu\mathrm{s}$ were $(||u_{64} - u_{128}||_2)/(||u_{128} - u_{256}||_2) = 2.40$, $(||v_{64} - v_{128}||_2)/(||v_{128} - v_{256}||_2) = 2.56$ and $(||w_{64} - w_{128}||_2)/(||w_{128} - w_{256}||_2) = 1.98$, which implies that the scheme is first-order accurate.

3. Results and discussion

In choosing the initial configuration, we start with a configuration that has a circular axial curve of radius r_0 and a uniform twist density $\Delta Lk/(2\pi r_0)$, and hence is an equilibrium solution of equations (2.3)–(2.8) in the absence of external force and moment, i.e. with $\mathbf{f} = 0$ and $\mathbf{n} = 0$. We perturb this configuration by varying the twist along the DNA while leaving the axial curve intact. In terms of cylindrical coordinates (r, θ, z) with unit vectors $(\mathbf{r}(\theta), \boldsymbol{\theta}(\theta), \mathbf{z})$, the initial configuration becomes

$$\mathbf{X}(s) = r_0(\cos\beta)\mathbf{r}\left(\frac{s}{r_0}\right), \tag{3.1}$$

$$\mathbf{D}^3(s) = (\cos\beta)\boldsymbol{\theta}\left(\frac{s}{r_0}\right) + (\sin\beta)\,\mathbf{z}, \tag{3.2}$$

$$\mathbf{E}(s) = -(\sin\beta)\boldsymbol{\theta}\left(\frac{s}{r_0}\right) + (\cos\beta)\mathbf{z}, \tag{3.3}$$

$$\mathbf{D}^1(s) = \cos\left(\Delta Lk\frac{s}{r_0} + g(s)\right)\mathbf{E}(s) + \sin\left(\Delta Lk\frac{s}{r_0} + g(s)\right)\mathbf{r}\left(\frac{s}{r_0}\right) \tag{3.4}$$

and $\quad \mathbf{D}^2(s) = -\sin\left(\Delta Lk\frac{s}{r_0} + g(s)\right)\mathbf{E}(s) + \cos\left(\Delta Lk\frac{s}{r_0} + g(s)\right)\mathbf{r}\left(\frac{s}{r_0}\right), \quad$ (3.5)

where

$$\sin\beta = -\frac{a_3\Delta Lk}{br_0^2 + a_3 - a}, \quad 0 \leq s \leq 2\pi r_0,$$

and

$$g(s) = \sum_m \epsilon_m \sin\frac{ms}{r_0}. \tag{3.6}$$

Note that integer-valued ΔLk implies that the triad will be continuous at $s = 0$, which is the same point as $s = 2\pi r_0$. The vector $\mathbf{E}(s)$ is a useful reference vector orthogonal to $\mathbf{D}^3$ within the plane spanned by $\boldsymbol{\theta}$ and $\mathbf{z}$. The charges are located on the axis at the discretization points. As each material point of the discretized immersed rod corresponds to a base pair of the circular DNA, the spacing between them is 0.34 nm.
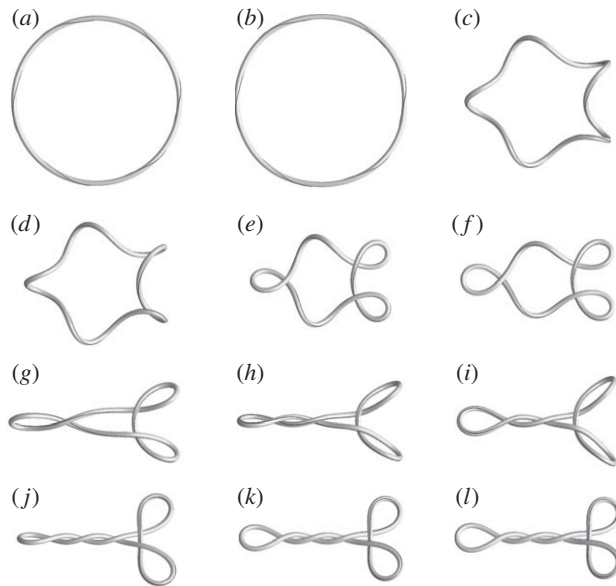
Figure 2. Example of a trajectory of a DNA minicircle with 600 bp, $C_s = 0.1$ M, $\Delta Lk = 6$ and other parameters as in table 1. Rapid equilibration of the twist density accompanied by a small perturbation of the axial curve $(a–b)$, is followed by a collapse of the circle through (c) and (d) to the point of first 'contact' (e) at which the DNA comes to close proximity and the motion abruptly slows down, continued through one or several intermediate configurations with non-increasing number of terminal loops and the creation of additional contacts $(f–j)$, and finally a slow convergence to a locally stable equilibrium accompanied by writhe relaxation $(j–l)$. (a) $t = 0$ μs; (b) $t = 0.2$ μs; (c) $t = 1.8$ μs; (d) $t = 2$ μs; (e) $t = 2.6$ μs; (f) $t = 3$ μs; (g) $t = 3.6$ μs; (h) $t = 4$ μs; (i) $t = 4.8$ μs; (j) $t = 15.2$ μs; (k) $t = 30$ μs; and (l) $t = 64$ μs.

The use of a circular initial configuration is standard in studies of DNA supercoiling, and corresponds to the situation in which a sudden change in the stress-free value of twist density pushes a stable circular minicircle above the instability threshold. This can be accomplished experimentally, for example, by adding intercalating agents to the solution.

We study the dynamics of initially circular DNA with excess link ΔLk fixed at a value between 1 and 6 and the molar salt concentration C_s fixed at 0.01, 0.05 or 0.1 M. Regardless of ΔLk, C_s and the initial perturbation, the majority of DNA trajectories we computed progressed through four characteristic phases described in figure 2.

(a) Dependence of limiting configurations on ΔLk and C_s

We first explore the dependence of trajectories and limiting configurations on ΔLk and C_s while the initial perturbation is held fixed. For $\Delta Lk = 1$, the circular configuration is stable even in the absence of electrostatics (Coleman & Swigon 2000). A familiar result in the theory of inextensible, unshearable elastic rods states that the circular equilibrium configuration is unstable if ΔLk exceeds a critical value $\Delta Lk^* = (a/a_3)\sqrt{3}$ (Michell 1889; Goriely 2006). The equivalent critical value for a charged rod with $a_3/a = 0.67$ has been estimated
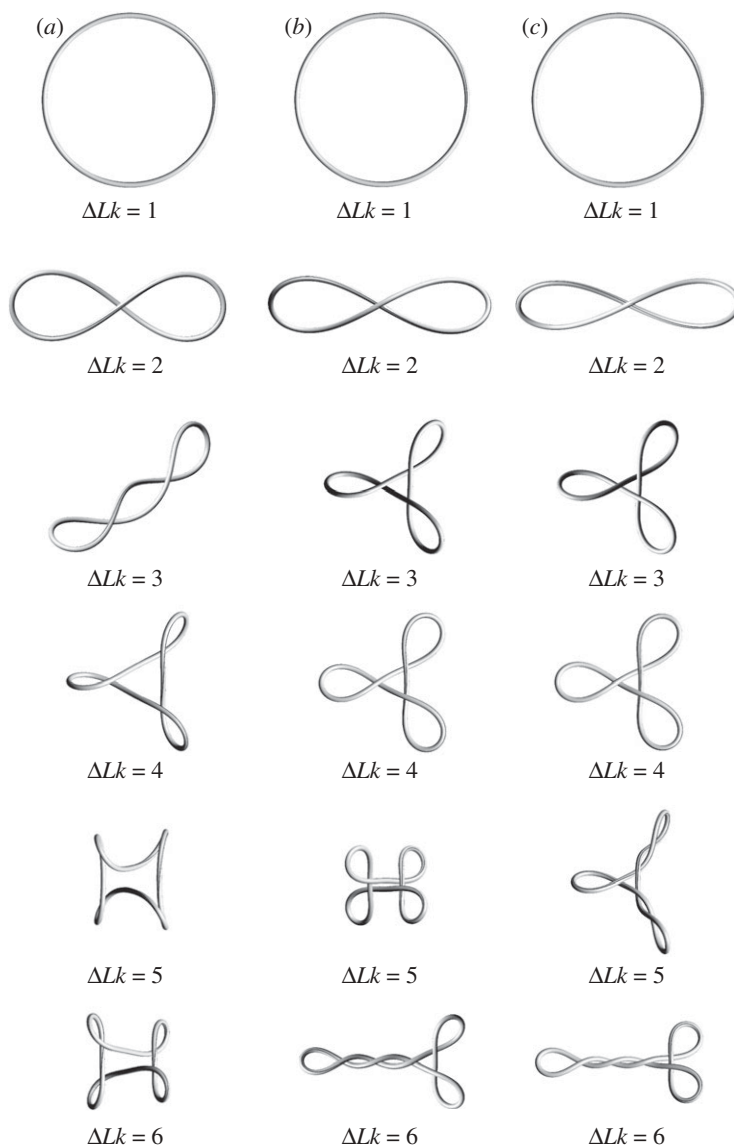
Figure 3. Limiting configurations of a 600 bp DNA minicircle with given value of the excess link ΔLk (i.e. imposed excess twist in a circular configuration) and salt concentration C_s, when started from identical initial perturbations (see text).(a) $C_s = 0.01\,\mathrm{M}$; (b) $C_s = 0.05\,\mathrm{M}$; (c) $C_s = 0.1\,\mathrm{M}$.

by Schlick *et al.* (1994) as a function of the ionic strength: $\Delta Lk^*(0.1\,\mathrm{M}) = 2.27$, $\Delta Lk^*(0.05\,\mathrm{M}) = 2.38$, $\Delta Lk^*(0.01\,\mathrm{M}) = 2.81$, $\Delta Lk^*(0.005\,\mathrm{M}) = 3.25$. We find that for our choice of $a_3/a = 1.4$, the circular configuration with $\Delta Lk = 2$ is unstable for $C_s \geq 0.01\,\mathrm{M}$. Furthermore, we find that $\Delta Lk^*(0.005\,\mathrm{M}) > 2$ and $\Delta Lk^*(0.001\,\mathrm{M}) > 3$.

When the circular state is unstable, the DNA deforms into a supercoiled configuration. Each column in figure 3 depicts limiting steady-state equilibrium configurations at specified values of excess link and salt concentration when the initial perturbation is chosen in accord with equation (3.6) with $\epsilon_1 = 1$, and $\epsilon_m = 0$
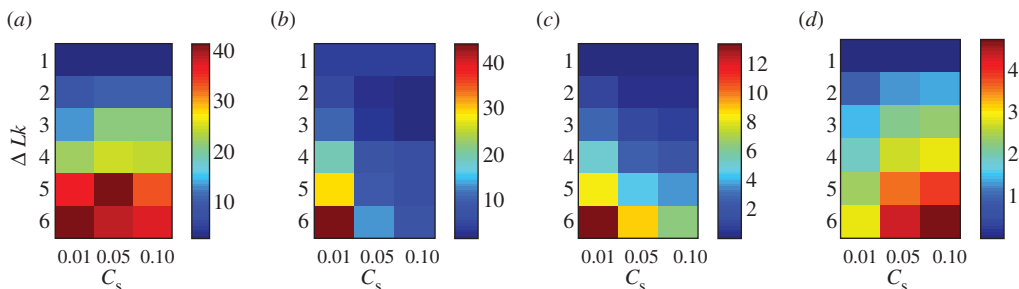
Figure 4. Energies (kT) and writhe for the configurations in figure 3. (a) E_{bending} (kT), (b) E_{twisting} (kT), (c) $\Delta E_{\text{electro}}$ (kT) and (d) Wr.

for $m \geq 2$. (Although each of these configurations is locally stable, they should not be viewed as the minimum energy configurations for there may be other configurations at the same value of ΔLk with even lower energy.)

The shapes of equilibrium configurations, supercoiled plasmids can be classified according to their symmetry (Coleman & Swigon 2000). In the absence of electrostatics, the minimum elastic-energy configuration for any value of excess link has the D_2 symmetry group (dihedral group of order 2) with three axes of rotational symmetry. Additional stable configurations with higher symmetries $(D_3, D_4,$ and so on) can be found for larger values of excess link. There are two types of supercoiled configurations: *plectonemically* supercoiled configurations have a small number of terminal loops and large two-ply plectonemic regions in which two helical DNA segments run in parallel. *Toroidally* supercoiled configurations have multiple terminal loops and DNA segments at the points of self-contact run transversally. The distinction is meaningless for $\Delta Lk < 3$. In figure 3, among the limiting configurations with $\Delta Lk \geq 3$ those with $(\Delta Lk, C_{\text{s}}) =$ $(3, 0.01\,\text{M})$, $(5, 0.1\,\text{M})$, $(6, 0.05\text{M})$ and $(6, 0.1\,\text{M})$ are plectonemically supercoiled, while the remaining ones are toroidally supercoiled.

The shapes of limiting configurations at high salt resemble those found for elastic rods without electrostatic repulsion (Coleman & Swigon 2000). The DNA at low salt has the tendency to limit the total extent in close contact, which results in a preference for toroidal supercoiling.

In figure 4, we compare the bending, twisting and electrostatic energies of configurations in figure 3. (The electrostatic energies are shown as a difference from the electrostatic energy of the circle at the same C_{s}.) Bending energy increases with ΔLk, but does not vary much with salt concentration. On the other hand, the twisting energy is independent of ΔLk at medium and high salt concentration, but depends strongly on ΔLk at low salt concentration. The differences in electrostatic energy among the configurations are much smaller than the differences in either bending or twisting energy—there is only a $6.43kT$ increase in electrostatic energy at $C_{\text{s}} = 0.1\,\text{M}$ as ΔLk varies from 1 to 6, although the configurations vary substantially; the bending energy, for example, changes by $34.52kT$. This reflects the charge screening—charges that are located more than several Debye lengths apart (which, in this case, equals $\kappa^{-1} = 10\,\text{Å}$) do not interact with each other. Writhe increases monotonically with both increasing ΔLk and increasing C_{s}.
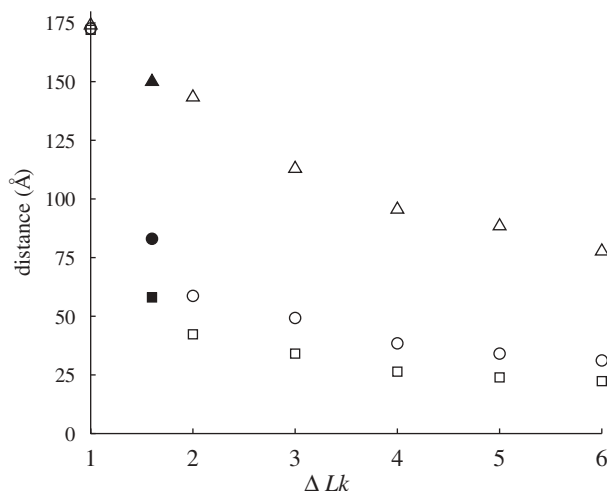
Figure 5. Distance of closest approach versus ΔLk for the configurations in figure 3 (open symbols). Solid symbols correspond to experimental estimates of the effective DNA diameter (Rybenkov *et al.* 1993) from DNA knotting experiments. Open triangles, $C_s = 0.01$ M; open circles, $C_s = 0.05$ M; open squares, $C_s = 0.1$ M.
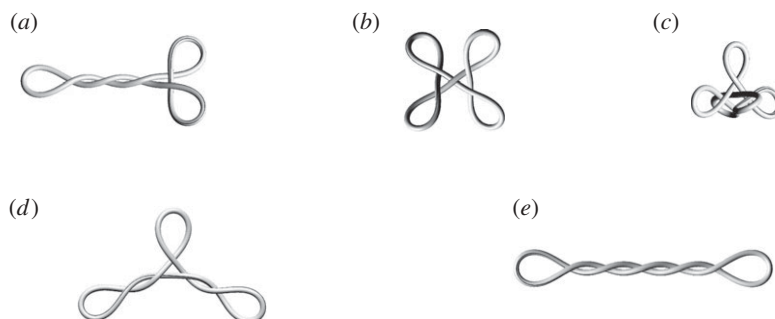
The stretching energy (not shown) plays a minor role, in accord with observations of Westcott *et al.* (1997), who showed that supercoiling dynamics of DNA is not much affected by DNA extensibility.

To assess the compaction of the supercoiled molecule, we measured the *distance of closest approach*, i.e. the closest distance between the centre of a given base pair and the centre of another base pair that has at least 20 base pairs separation along the axis of the DNA (figure 5). The distance of closest approach decreases with increasing molar salt concentration and increasing ΔLk, as a result of increased supercoiling and decreased electrostatic repulsion. The distance of closest approach can be compared in figure 5 with experimental estimates of the effective DNA radius, based on measurements of knotting probability in the absence of supercoiling (Rybenkov *et al.* 1993). In those experiments, no supercoiling was imposed and hence we plot their estimated values at an arbitrary value $\Delta Lk = 1.6$. The values of closest approach we calculate are smaller than the effective DNA diameter at the same ionic strength because supercoiling induces forces that push the DNA into closer proximity. The values of plectonemic radius versus ionic strength reported by Ubbink & Odjik (1999) and Rybenkov *et al.* (1997) are about twice as large as those we find, most likely because our values are for equilibrium configurations and do not account for thermal fluctuations that would tend to increase the plectonemic radius.

Numerical results also show that for a fixed salt concentration, the distance between two adjacent base pairs (i.e. the stretching of the DNA) is essentially constant, regardless of different initial twist number ΔLk (in accord with Westcott *et al.* 1997) and it slightly increases as the salt concentration decreases. Figure 6 shows five different projections of the equilibrium configurations for $(\Delta Lk, C_s) = (5, 0.01 \, \text{M})$ and $(5, 0.05 \, \text{M})$, to demonstrate that there are no actual self-contact points anywhere along the configuration as the distance of closest approach is larger than D.

(a)

(b)

Figure 6. Different views of the limiting configuration for (*a*) $(\Delta Lk, C_{\mathrm{s}}) = (5, 0.01\,\mathrm{M})$ and (*b*) $(\Delta Lk, C_{\mathrm{s}}) = (5, 0.05\,\mathrm{M})$. There is no self-contact in any of the configurations.

(a)   (b)   (c)

(d)   (e)

energy (kT)	(*a*)	(*b*)	(*c*)	(*d*)	(*e*)
E_{bending}	37.6	45.6	62.0	38.7	28.8
E_{twisting}	7.7	11.2	7.2	7.9	6.8
E_{electro}	348.2	347.3	346.8	348.0	348.1
E_{total}	400.8	411.7	423.3	401.9	391.2
Wr	4.66	4.39	4.70	4.65	4.75

Figure 7. Locally stable equilibrium configurations for $(\Delta Lk, C_{\mathrm{s}}) = (6, 0.1\,\mathrm{M})$ obtained as limiting configurations of trajectories starting at different perturbations of the circular configuration.

In the theory of elastic rods with self-contact, multiple locally stable equilibrium configurations exist for $\Delta Lk > 1$ (Coleman & Swigon 2000; Coleman *et al.* 2000). In the presence of electrostatics, two types of locally stable equilibria (lobed and interwound) were found by Schlick *et al.* (1994) for several values of ΔLk. It is not known, however, how many local equilibria exist or whether they all can be attained by a path from a perturbed circular configuration, i.e. whether the domain of attraction of each local equilibrium extends up to a neighbourhood of the circular equilibrium. We have examined this question by sampling over different perturbations of circular configurations with excess link $\Delta Lk = 6$ and the molar salt concentration $C_{\mathrm{s}} = 0.1\,\mathrm{M}$, and observed which configurations appeared as the limits of corresponding trajectories. Our search led to a total of five distinct limiting configurations shown in figure 7. Among those are the 2-loop plectoneme, which minimizes the total energy, two types of 3-loop configurations, one 4-loop configuration and one 5-loop configuration. The 4-loop configuration was the most commonly occurring limiting configuration.
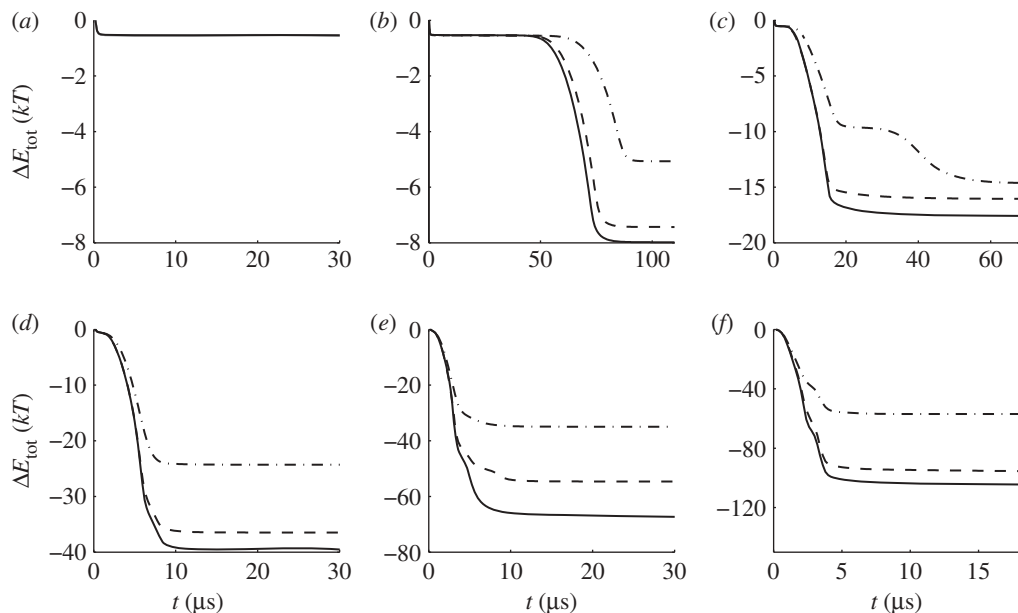
Figure 8. Decrease in total energy from initial value versus time for trajectories leading to the configurations in figure 3. Excess link is as indicated, the ionic strength is 0.01 M (dashed-dotted line), 0.05 M (dashed line) and 0.1 M (solid line). (*a*) $\Delta Lk = 1$, (*b*) $\Delta Lk = 2$, (*c*) $\Delta Lk = 3$, (*d*) $\Delta Lk = 4$, (*e*) $\Delta Lk = 5$ and (*f*) $\Delta Lk = 6$.

(*b*) *Dynamics of transitions*

The time of transition from the perturbed circle to a stable equilibrium configuration for the cases shown in figure 3 varies greatly with ΔLk and C_s. The dynamics of each trajectory that produced a configuration in figure 3 can be followed on the plots of total energy, kinetic energy and writhe versus time in figures 8–10.

As expected, for every transition path, the total energy decreases with time due to the strong dissipation in the system. The plateaus in the graphs of total energy coincide with local minima in the kinetic energy and correspond to transient states near unstable equilibrium configurations. The transient states resemble the unstable equilibria of elastic rods with self-contact in the absence of electrostatics, which can be found using explicit solutions of the governing equations of Kirchhoff's theory of rods (Coleman & Swigon 2000; Coleman *et al.* 2000).

The time of convergence to the limiting configuration can be estimated from the graphs of writhe versus t (figure 10) as the largest t for which $|W(t) - W^\infty| > \delta$, where δ is some small positive number, say 0.01. The convergence time for each trajectory that produced a configuration in figure 3 can be found in table 2. The convergence time is longest for configurations with $\Delta Lk = 2$ regardless of ionic strength. For $\Delta Lk > 3$, the convergence times differ depending on whether the limiting configuration shows plectonemic or toroidal supercoiling. Toroidally supercoiled configurations are attained much faster at around 10.1 μs on average, independent of ΔLk and C_s. Plectonemic configurations are attained on average in 47.3 μs.
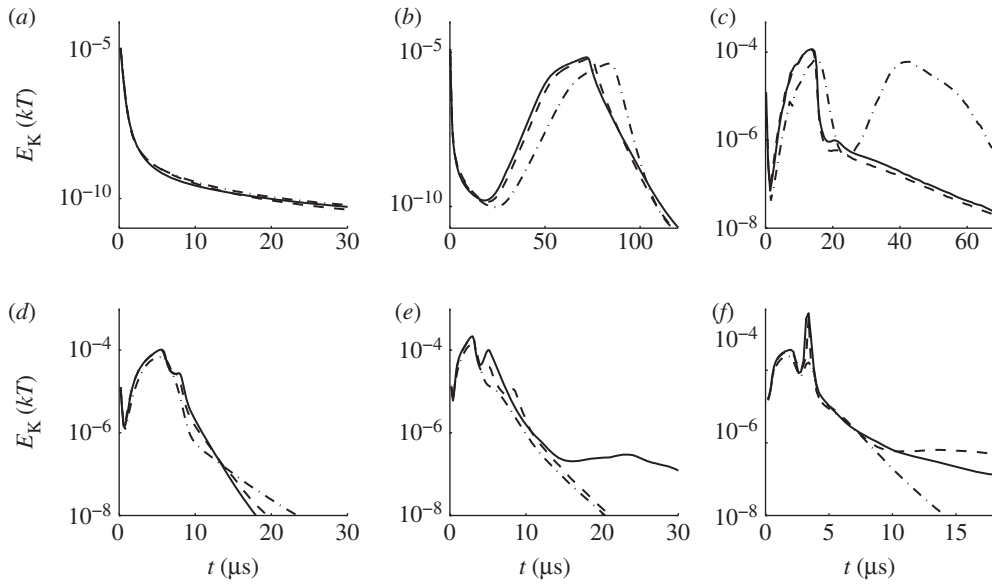
S. Lim et al.

Figure 9. Kinetic energy versus time for trajectories leading to the configurations in figure 3. Excess link is as indicated, ionic strength is 0.01 M (dashed-dotted line), 0.05 M (dashed line) and 0.1 M (solid line). (*a*) $\Delta Lk = 1$, (*b*) $\Delta Lk = 2$, (*c*) $\Delta Lk = 3$, (*d*) $\Delta Lk = 4$, (*e*) $\Delta Lk = 5$ and (*f*) $\Delta Lk = 6$.
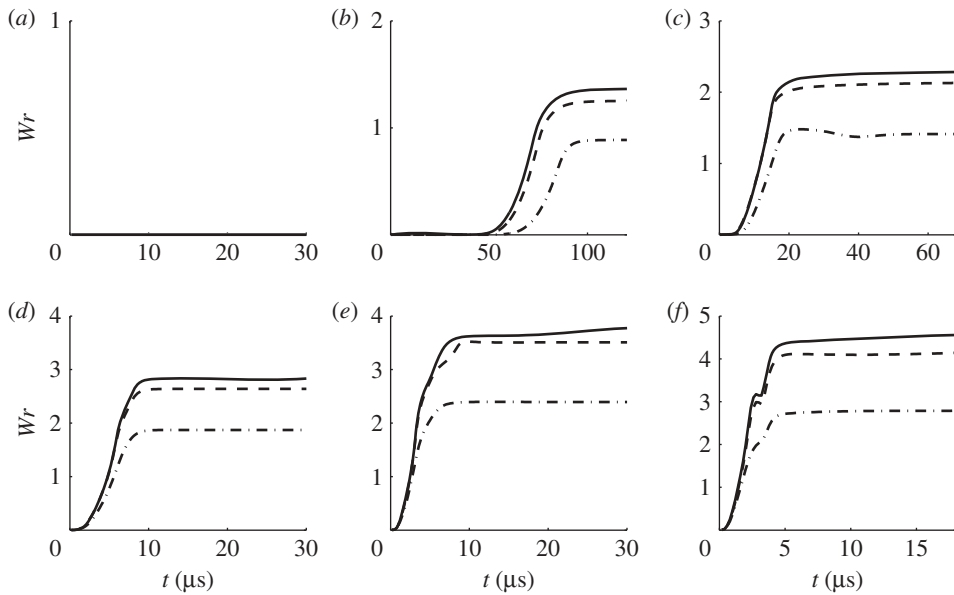

Figure 10. Writhe versus time for trajectories leading to the configurations in figure 3. Excess link is as indicated, ionic strength is 0.01 M (dashed-dotted line), 0.05 M (dashed line) and 0.1 M (solid line). (*a*) $\Delta Lk = 1$, (*b*) $\Delta Lk = 2$, (*c*) $\Delta Lk = 3$, (*d*) $\Delta Lk = 4$, (*e*) $\Delta Lk = 5$ and (*f*) $\Delta Lk = 6$.
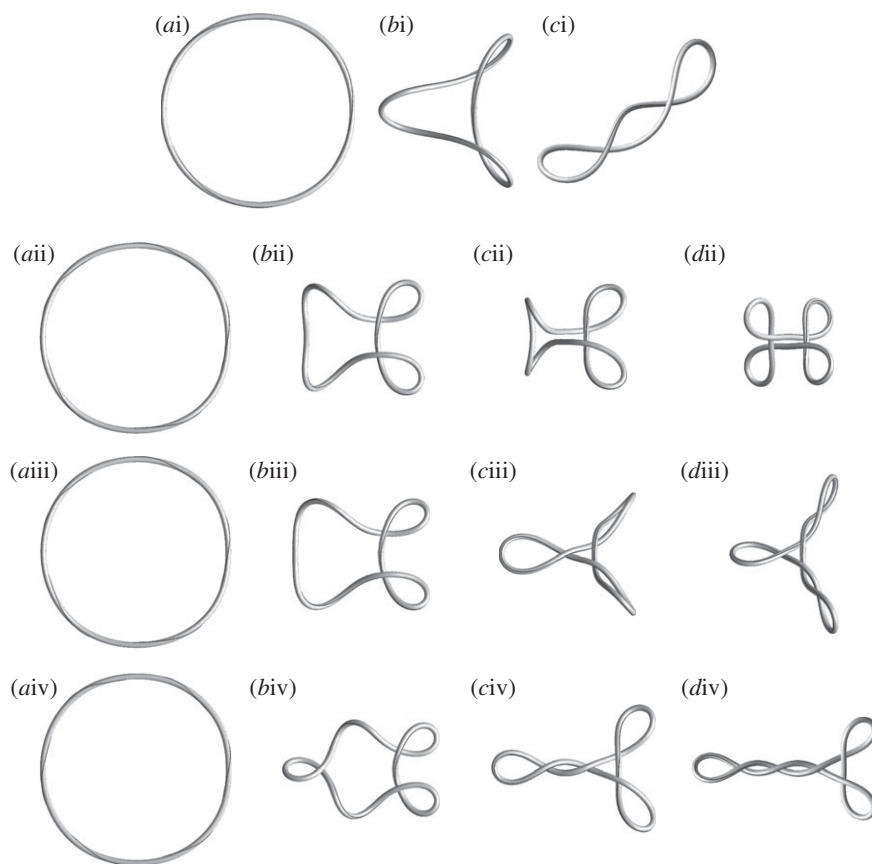
Figure 11. Equilibria on a transition path. The last configuration in each row is locally stable, all others are transient states. Parameters for each row, top to bottom: $(\Delta Lk, C_s) = (3, 0.01\,\mathrm{M}), (5, 0.05\,\mathrm{M}), (5, 0.1\,\mathrm{M})$ and $(6, 0.05\,\mathrm{M})$. (*a*i) $t = 1.6\,\mu s$; (*b*i) $t = 25.6\,\mu s$; (*c*i) $t = 100\,\mu s$; (*a*ii) $t = 0.4\,\mu s$; (*b*ii) $t = 4.4\,\mu s$; (*c*ii) $t = 7.4\,\mu s$; (*d*ii) $t = 100\,\mu s$; (*a*iii) $t = 0.4\,\mu s$; (*b*iii) $t = 4.0\,\mu s$; (*c*iii) $t = 15.6\,\mu s$; (*d*iii) $t = 100\,\mu s$; (*a*iv) $t = 0.2\,\mu s$; (*b*iv) $t = 2.8\,\mu s$; (*c*iv) $t = 10.6\,\mu s$; (*d*iv) $t = 100\,\mu s$.

Table 2. Writhe convergence time (μs) for trajectories leading to the configurations in figure 3.

ΔLk	C_s		
	0.01 M	0.05 M	0.1 M
2	97.8	98.2	101.4
3	49.2	63.6	65.2
4	10.2	10.2	10.6
5	8.6	10.6	50.6
6	10.4	45.8	43.4

The most prominent transient state, found as a local minimum in the plot of the kinetic energy in figure 9, can be seen in the trajectory for $(\Delta Lk, C_s) = (3, 0.01\,\mathrm{M})$. Other transient states are in $(\Delta Lk, C_s) = (5, 0.05\,\mathrm{M})$, $(5, 0.1\,\mathrm{M})$ and $(6, 0.05\,\mathrm{M})$ (figure 11).

The fastest transition is observed for $\Delta Lk = 1$ as that trajectory involves only equilibration of the twist along the DNA and no deformation of the axial curve. In this case, the relaxation of kinetic energy obeys a power law, i.e. $E_K \sim t^{-m}$, with $m = 1.8 \pm 0.1$, which is independent of C_s.

For $\Delta Lk = 2$, the transition paths are also independent of C_s. They start with an equilibration of twist and approach to the unstable circular configuration, followed by a buckling transition along the branch of configurations with D_2 symmetry and terminating at a figure 8 configuration.

For $\Delta Lk = 3$, the transition paths depend on C_s. After the initial twist equilibration, all three trajectories proceed towards the unstable equilibrium similar to the configuration shown in figure 11bi. Then, for $C_s = 0.01\,\mathrm{M}$, the trajectory continues towards a plectonemic configuration in figure 11ci. For $C_s = 0.05\,\mathrm{M}$ and $0.1\,\mathrm{M}$, however, the trajectory continues towards the configuration with D_3 symmetry, seen in figure 3. This transition is slower than the one for $C_s = 0.01\,\mathrm{M}$, but because it does not dwell in a transient state, the final writhe is attained at about the same time (table 2).

For $\Delta Lk = 4$, the transition paths are again essentially independent of the ionic strength and similar to the path for $(\Delta Lk, C_s) = (3, 0.05\,\mathrm{M})$, with no significant dwell time near any locally stable equilibrium.

For $\Delta Lk = 5$, the transition paths depend on C_s. After the initial twist equilibration, the trajectory for $C_s = 0.01\,\mathrm{M}$ proceeds directly towards a configuration with four terminal loops. For $C_s = 0.05\,\mathrm{M}$ and $0.1\,\mathrm{M}$, the trajectories proceed to a transient shown in figure 11$b$ii and 11$b$iii. Then, for $C_s = 0.05\,\mathrm{M}$, the trajectory proceeds towards a second transient state figure 11$c$ii and continues towards a limiting configuration with four lobes. For $C_s = 0.1\,\mathrm{M}$, however, the trajectory departs towards a transient state figure 11$c$iii with three terminal loops and continues with a slow equilibration of the writhe towards the final configuration with two plectonemic loops.

Finally, for $\Delta Lk = 6$, the transition paths again depend on C_s. After the initial twist equilibration, the trajectory for $C_s = 0.01\,\mathrm{M}$ proceeds directly towards a configuration with four terminal loops, similarly as for $\Delta Lk = 4$. For $C_s = 0.05\,\mathrm{M}$ and $0.1\,\mathrm{M}$, the transition proceeds along a path similar to (or exactly like) the one in figure 2 with one transient state at $t = 2.6\,\mathrm{\mu s}$ (for $C_s = 0.1\,\mathrm{M}$). The final equilibration of the writhe is again a slow process because of the presence of a long plectonemic loop.

Figure 11$a$ii–$d$ii and 11$a$iii–$d$iii illustrates the remarkable sensitivity of the supercoiling process to ionic strength, whereby a small difference in salt concentration causes the system to depart the same transient configuration along markedly different paths.

With the exception of the initial twist relaxation, the approach of a configuration $\mathbf{X}(t)$ to a local equilibrium $\mathbf{X}_{eq}$ is close to exponential, and hence we can define the *relaxation time* of a local equilibrium, τ, as $||\mathbf{X}(t) - \mathbf{X}_{eq}|| \approx \mathrm{e}^{-t/\tau}$. The relaxation times can be estimated from the graph of the kinetic energy, which scales as $\mathrm{e}^{-2t/\tau}$, when equilibrium is approached. Relaxation times for the limiting configurations with $\Delta Lk > 1$, shown in figure 3, are given in table 3. They are computed for the transition phase after which no further contacts between DNA segments are formed and no further rearrangement of contacts occurs. With the exception of $\Delta Lk = 4$, for which we observe the fastest relaxation times, for any other given ΔLk,

Table 3. Relaxation time (μs) for the configurations in figure 3.

ΔLk	C_s		
	0.01 M	0.05 M	0.1 M
2	1.0	1.7	1.9
3	3.3	7.3	7.3
4	2.1	1.1	0.9
5	1.1	1.2	3.0
6	0.8	2.6	3.1

the relaxation time gets larger as salt concentration increases. The toroidally supercoiled configurations have shorter relaxation times than the plectonemically supercoiled ones.

4. Summary and conclusion

In this paper, we present an improved generalized IB method for simulation of the dynamics of elastic rods in a fluid. By including electrostatic repulsion and steric (hard-core) interaction between rod segments, we completely eliminate any self-penetration of the modelled rod during simulations and assure the conservation of linking number. The model can be applied to macroscopic structures, such as underwater cables, ropes and fishing lines (charged or not), to cellular components, such as bacterial filaments and microtubules, and to short semiflexible polymers, such as DNA.

We here focus on supercoiling of twisted DNA rings, and explore the dependence of the dynamical trajectories and limiting configurations on the excess link, ionic strength and perturbation. Our goal is to obtain a better idea about the kinetics of supercoiling processes in short molecules, motivated by the possibility that loop-formation kinetics, not just equilibrium, may be important in biological processes in which binding and unbinding of proteins happens on fast time scales. We confirm the earlier findings (Schlick *et al.* 1994; Westcott *et al.* 1995) that the type of limiting configuration is influenced by ionic strength in which higher salt gives rise to plectonemic supercoiling, while low salt gives rise to toroidal supercoiling. In all the limiting structures we found, the repulsion is sufficiently strong that the DNA surface remains free of direct contact.

We find that the dynamics of the ring is overdamped and that the time of transition from the circle to a supercoiled configuration can vary greatly depending on excess link and ionic strength, and that the transition slows down at various times as the configuration approaches unstable equilibria, with characteristic plateaus in the total energy. Similar plateaus were observed in the dynamics of elastic rods with self-contact (Goyal *et al.* 2008). The dwell time near such equilibria is of the order of 1–10 μs, which is enough time for a protein to bind and connect DNA segments that are in proximity. The transition paths are sensitive to ionic strength—small changes in ionic strength may cause divergence of the trajectories in the neighbourhood of transient states.

We confirm the existence of multiple locally stable configurations for the given ionic strength and excess link, and find that each such configuration can be attained with an appropriate initial perturbation of the circle. Our search

recovered all locally stable equilibria known from the theory of elastic rods with self-contact (Coleman & Swigon 2000), and hence, we conjecture that any locally stable equilibrium configuration of a closed rod can be attained from the circular configuration with the same excess link by a dynamical trajectory that starts with an appropriate initial perturbation in twist density.

Our findings on the departure from the circular configuration are in accord with the results from perturbation analyses of looping and ring collapse transitions (Goriely & Tabor 1997) and numerical analyses of supercoiling of DNA plasmids (Klapper 1996), in the sense that if the excess link is large enough, the departure from the unstable twisted circular configuration is fastest along the mode with four loops. It is not the only unstable mode and other modes can be excited with different perturbations—these modes generally lead to other locally stable configurations.

At the length scales corresponding to the size of our minicircles, random fluctuations, not accounted by our method, have an additional effect on DNA supercoiling dynamics, primarily by enabling transitions between various locally stable configurations and perturbing the configurations in such a way that the probability of occurrence of any configuration is given by the Boltzmann distribution. Stochastic dynamics of 1000–1500 bp DNA plasmids has been studied using Brownian dynamics with excluded volume (Chirico & Langowski 1994) and electrostatics (Jian *et al.* 1998). The average relaxation times for writhe reported in Chirico & Langowski (1994) are 6 µs for $\Delta Lk = 4$ and 3.5 µs for $\Delta Lk = 6$, those reported in Jian *et al.* (1998) are 20 µs for $\Delta Lk = 4$ and 10 µs for $\Delta Lk = 5.5$, both at $C_s = 0.01$ M. Our results indicate that relaxation time depends on the limiting configuration, but is in the range of 0.8–8 µs. Thermal fluctuations can be accounted for in the framework of the generalized IB method by adding a random force with a Boltzmann distribution acting on the fluid (Atzberger *et al.* 2007). We plan to combine electrostatic repulsion and thermal fluctuations in a future implementation of the generalized IB method.

The theory of counterion condensation, employed in this paper, is based on approximations that are valid only in the limit of low salt concentrations and for an infinitely long, straight polyion. Although the theory has been shown to provide good estimates of DNA repulsive forces up to the values of ionic strength considered here, a more accurate and potentially interesting extension of the current work would be to account explicitly for the dynamics of ion distribution and its interaction with the DNA. It is possible that the ions would localize near the plectonemic regions of DNA, which would make configurations showing such regions energetically favourable.

References

Antman, S. 1995 *Nonlinear theories of elasticity.* New York, NY: Springer.

Atzberger, P. J., Kramer, P. R. & Peskin, C. S. 2007 A stochastic immersed boundary method for fluid-structure dynamics at microscopic length scales. *J. Comp. Phys.* **224**, 1255–1292. (doi:10.1016/j.jcp.2006.11.015)

Bates, A. D. & Maxwell, A. 1993 *DNA topology*. Oxford, UK: Oxford University Press.

Baumann, C. G., Smith, S. B., Bloomfield, V. A. & Bustamante, C. 1997 Ionic effects on the elasticity of single DNA molecules. *Proc. Natl Acad. Sci. USA* **94**, 6185–6190. (doi:10.1073/pnas.94.12.6185)

Benham, C. J. 1989 Onset of writhing in circular elastic polymers. *Phys. Rev. A* **39**, 2582–2586. (doi:10.1103/PhysRevA.39.2582)

Biton, Y. Y. & Coleman, B. D. 2010 Theory of the influence of changes in salt concentration on the configuration of intrinsically curved, impenetrable, rod-like structures modeling DNA minicircles. *Int. J. Nonlin. Mech.* **45**, 735–755. (doi:10.1016/j.ijnonlinmec.2010.05.004)

Biton, Y. Y., Coleman, B. D. & Swigon, D. 2007 On bifurcations of equilibria of intrinsically curved, electrically charged, rod-like structures that model DNA molecules in solution. *J. Elasticity* **87**, 187–210. (doi:10.1007/s10659-007-9103-7)

Brutzer, H., Luzzietti, N., Klaue, D. & Seidel, R. 2010 Energetics at the DNA supercoiling transition. *Biophys. J.* **98**, 1267–1276. (doi:10.1016/j.bpj.2009.12.4292)

Calladine, C. R., Drew, H. R., Luisi, B. F. & Travers, A. A. 2004 *Understanding DNA: the molecule and how it works*, 3rd edn. London, UK: Elsevier Academic Press.

Chirico, G. & Langowski, J. 1994 Kinetics of DNA supercoiling studied by Brownian dynamics simulation. *Biopolymers* **34**, 415–433. (doi:10.1002/bip.360340313)

Clauvelin N., Audoly, B. & Neukirch, S. 2009 Elasticity and electrostatics of plectonemic DNA. *Biophys. J.* **96**, 3716–3723. (doi:10.1016/j.bpj.2009.02.032)

Coleman B. D. & Swigon, D. 2000 Theory of supercoiled elastic rings with self contact and its application to DNA plasmids. *J. Elasticity* **60**, 171–221. (doi:10.1023/A:1010911113919)

Coleman, B. D., Tobias, I. & Swigon, D. 1995 Theory of the influence of end conditions on self-contact in DNA loops. *J. Chem. Phys.* **103**, 9101–9109. (doi:10.1063/1.470021)

Coleman, B. D., Swigon, D. & Tobias, I. 2000 Elastic stability of DNA configurations: II. Supercoiled plasmids with self contact. *Phys. Rev. E* **61**, 759–770. (doi:10.1103/PhysRevE.61.759)

Dichmann, D. J., Li, Y. & Maddocks, J. H. 1996 Hamiltonian formulations and symmetries in rod mechanics. In *Mathematical approaches to biomolecular structure and dynamics* (eds J. P. Mesirov, K. Schulten & D. Sumners). New York, NY: Springer.

Goriely, A. 2006 Twisted elastic rings and the rediscoveries of Michell's instability. *J. Elasticity* **84**, 281–299. (doi:10.1007/s10659-006-9055-3)

Goriely, A. & Tabor, M. 1997 Nonlinear dynamics of filaments I. Dynamical instabilities. *Physica D* **105**, 20–44. (doi:10.1016/S0167-2789(96)00290-4)

Goyal, S., Perkins, N. C. & Lee, C. L. 2005 Nonlinear dynamics and loop formation in Kirchhoff rods with implications to the mechanics of DNA and cables. *J. Comp. Phys.* **209**, 371–389. (doi:10.1016/j.jcp.2005.03.027)

Goyal, S., Perkins, N. C. & Lee, C. L. 2008 Non-linear dynamic intertwining of rods with self-contact. *Int. J. Nonlin. Mech.* **43**, 65–73. (doi:10.1016/j.ijnonlinmec.2007.10.004)

Horowitz, D. S. & Wang, J. C. 1984 Torsional rigidity of DNA and length dependence of the free energy of DNA supercoiling. *J. Mol. Biol.* **173**, 75–91. (doi:10.1016/0022-2836(84)90404-2)

Jian, H., Schlick, T. & Vologodskii, A. 1998 Internal motion of supercoiled DNA: Brownian dynamics simulations of site juxtaposition. *J. Mol. Biol.* **284**, 287–296. (doi:10.1006/jmbi.1998.2170)

Klapper, I. 1996 Biological applications of the dynamics of twisted elastic rods. *J. Comput. Phys.* **125**, 325–337. (doi:10.1006/jcph.1996.0097)

Le Bret, M. 1979 Catastrophic variation of twist and writhing of circular DNAs with constraint? *Biopolymers* **18**, 1709–1725. (doi:10.1002/bip.1979.360180710)

Le Bret, M. 1984 Twist and writhing in short circular DNAs according to first-order elasticity. *Biopolymers* **23**, 1835–1867. (doi:10.1002/bip.360231004)

Lim, S., Ferent, A., Wang, X. S. & Peskin, C. S. 2008 Dynamics of a closed rod with twist and bend in fluid. *SIAM J. Scientific Comput.* **31**, 273–302. (doi:10.1137/070699780)

Manning, G. S. 1978 The molecular theory of polyelectrolyte solutions with applications to the electrostatic properties of polynucleotides. *Q. Rev. Biophys.* **2**, 179–246. (doi:10.1017/S0033583500002031)

Michell, J. H. 1889 On the stability of a bent and twisted wire. *Messenger Math.* **11**, 181–184.

Odijk, T. 1977 Polyelectrolytes near the rod limit. *J. Polym. Sci., Polym. Phys. Ed.* **15**, 477–483. (doi:10.1002/pol.1977.180150307)

Peskin, C. S. 1972 Flow patterns around heart valves: a numerical method. *J. Comput. Phys.* **10**, 252–271. (doi:10.1016/0021-9991(72)90065-4)

Peskin C. S. 2002 *The immersed boundary method.* Cambridge, UK: Cambridge University Press.

Peskin, C. S. & McQueen, D. M. 1996 Fluid dynamics of the heart and its valves. In *Case studies in mathematical modeling: ecology, physiology, and cell biology* (eds H. G. Othmer, F. R. Adler, M. A. Lewis & J. C. Dallon), pp. 309–337. Englewood Cliffs, NJ: Prentice-Hall.

Rybenkov, V. V., Cozzarelli, N. R. & Vologodskii, A. V. 1993 Probability of DNA knotting and the effective diameter of the DNA double helix. *Proc. Natl Acad. Sci. USA* **90**, 5307–5311. (doi:10.1073/pnas.90.11.5307)

Rybenkov, V. V., Cozzarelli, N. R. & Vologodskii, A. V. 1997 The effect of ionic conditions on the conformations of supercoiled DNA. I. Sedimentation analysis. *J. Mol. Biol.* **267**, 299–311. (doi:10.1006/jmbi.1996.0876)

Schlick, T., Li, B. & Olson, W. K. 1994 The influence of salt on the structure and energetics of supercoiled DNA. *Biophys. J.* **67**, 2146–2166. (doi:10.1016/S0006-3495(94)80732-5)

Skolnick, J. & Fixman, M. 1977 Electrostatic persistence length of a wormlike polyelectrolyte. *Macromolecules* **10**, 944–948. (doi:10.1021/ma60059a011)

Strick, T. R., Allemand, J. F., Bensimon, D., Bensimon, A. & Croquette, V. 1996 The elasticity of a single supercoiled DNA molecule. *Science* **271**, 1835–1837. (doi:10.1126/science.271.5257.1835)

Swigon, D. 2009 *The mathematics of DNA structure, mechanics, and dynamics.* IMA volumes in mathematics and its applications, vol. 150, pp. 293–320. Berlin, Germany: Springer.

Tobias, I., Coleman, B. D. & Olson, W. K. 1994 The dependence of DNA tertiary structure on end conditions: theory and implications for topological transitions. *J. Chem. Phys.* **101**, 10 990–10 996. (doi:10.1063/1.467849)

Ubbink, J. & Odjik, T. 1999 Electrostatic-undulatory theory of plectonemically supercoiled DNA. *Biophys. J.* **76**, 2502–2519. (doi:10.1016/S0006-3495(99)77405-9)

Westcott, T. P., Tobias, I. & Olson, W. K. 1995 Elasticity theory and numerical analysis of DNA supercoiling: an application to DNA looping. *J. Phys. Chem.* **99**, 17 926–17 935. (doi:10.1021/j100051a018)

Westcott, T. P., Tobias, I. & Olson, W. K. 1997 Modeling self-contact forces in the elastic theory of DNA supercoiling. *J. Chem. Phys.* **107**, 3967–3980. (doi:10.1063/1.474752)

White, J. H. 1969 Self-linking and the Gauss integral in higher dimensions. *Am. J. Math.* **91**, 693–728. (doi:10.2307/2373348)

White, J. H. 1989 An introduction to the geometry and topology of DNA structure. In *Mathematical methods for DNA sequences* (ed. M. S. Waterman). Boca Raton, FL: CRC Press.

Williams, L. D. & Maher III, L. J. 2000 Electrostatic mechanisms of DNA deformation. *Annu. Rev. Biophys. Biomol. Struct.* **29**, 497–521. (doi:10.1146/annurev.biophys.29.1.497)

Yang, Y., Tobias, I. & Olson, W. K. 1993 Finite element analysis of DNA supercoiling. *J. Chem. Phys.* **98**, 1673–1686. (doi:10.1063/1.464283)